Gas phase synthesis of fcc-cobalt nanoparticles†

Robert N. Grass and Wendelin J. Stark*

Received 23rd January 2006, Accepted 13th March 2006
First published as an Advance Article on the web 28th March 2006
DOI: 10.1039/b601013j

Air stable cobalt nanoparticles have been prepared continuously at a production rate of 30 g h^{-1} by a modified flame synthesis method under highly reducing conditions. Nanoparticles of 20–60 nm in diameter consisted of metallic face-centered-cubic cobalt. The metal particles were protected against oxidation by a surface layer of less than 1 nm of cobalt oxide. The material was highly magnetic exhibiting a high saturation magnetisation (>124 emu g^{-1}) together with a low (<100 Oe) coercivity. Experiments under varying fuel to oxygen ratio were combined with thermodynamic calculations to illustrate the necessity for highly reducing conditions and enhanced gas mixing to enable the formation of metallic cobalt nanoparticles in flames.

Introduction

The enhanced mechanical, electronic and magnetic properties[1] of metallic nanoparticles have triggered proposals for applications as high-density magnetic storage devices,[2] hall sensors,[3] soft magnetic materials exhibiting higher permeability or lower coercivity[4] and heterogeneous catalysts,[5] amongst others. Metallic cobalt nanoparticles have been available from wet-phase synthesis methods for more than 50 years,[6] today offering good control of product size and shape.[7] The wide range of synthetic, mainly liquid based, preparation methods offers access to cobalt nanoparticles of primary particle sizes starting from only several nanometers up to submicron sized materials. While most preparations result in particles of a broad particle size distribution, almost monodisperse distributions could be obtained from controlled reduction using specific additives.[8] However, in the case of oxides, the large scale production of nanoparticles at high purity preferably requires continuous gas-phase processes which avoid drying, follow-up treatment and purification of the products. Today flame aerosol processes are used commercially for the synthesis of more than 10 million metric tons of particles per year. They provide a route to a wealth of ceramic products,[9] salts[10] and composites for applications in optics,[11] electronics[12] and catalysis.[13] In comparison to other gas-phase methods using hot-wall reactors, laser or plasma synthesis,[14] flames use hydrocarbons as a low cost source of energy.

Most recently, a scalable[15] flame spray synthesis method was developed as a suitable tool to manufacture nanoparticles of metal oxides,[16] salts[17,18] and noble metals[19] from liquid precursors. Amongst others, the use of metal carboxylates[20] allowed the preparation of nanoparticles with narrow size distributions.[18] Extension of this process to the synthesis of cobalt nanoparticles would be most attractive. Prior investigations on the formation of carbon nanotubes,[21] carbon black and fullerenes or noble metals[22] in flames have shown that metals can coexist in sufficiently fuel rich flames. Cobalt,[23] iron[24] and copper[25] nanoparticles were used to catalyse the formation of carbon nanotubes and exclusively resulted in samples consisting of small metallic clusters embedded in a carbonaceous matrix and carbon-coated copper nanoparticles.

We therefore used a flame spray burner in an oxygen free atmosphere. Shielding through a porous tube allowed for enhanced gas mixing and operation under the required fuel-rich conditions to prepare carbon-free metallic cobalt nanoparticles. Experiments under varying atmospheres and thermodynamic calculations provided further insight into the formation of metallic cobalt nanoparticles in flames.

Experimental

Powder preparation

Precursor preparation. Cobalt 2-ethylhexanoate in mineral spirit (S.C. Soctec S. A., 12 wt% Co) was diluted 2 : 1 (weight/weight) with tetrahydrofuran (Fluka, tech.) and filtered (Satorius, fluted filter type 288) prior to use.

Conventional flame spray set-up. The Co-carboxylate-based precursor was fed (5 ml min^{-1}, HNP Mikrosysteme, micro annular gear pump mzr-2900) to a spray nozzle[26] (see ESI†) where it was dispersed by oxygen (5 l min^{-1}, PanGas tech.) and ignited by a premixed methane–oxygen flame (CH_4: 1.2 l min^{-1}, O_2: 2.2 l min^{-1}, PanGas tech.). The produced particles were separated from the off-gas using glass fiber filters (Schleicher & Schuell, GF6).

Reducing flame spray synthesis. The spray nozzle[26] was placed in a glove-box fed with nitrogen (PanGas, 5.0) which was recirculated by a vacuum pump (Busch, Seco SV1040CV) at about 20 m^3 h^{-1}. CO_2 and H_2O were continuously removed from the recycle stream using two adsorption columns, packed with zeolite 4A and 13X (Zeochem), respectively. To avoid the accumulation of CO, NO and other impurities in the glove-box atmosphere a purge gas stream continuously passed through

Institute for Chemical and Bioengineering, ETH Zurich, 8093, Zurich, Switzerland. E-mail: wendelin.stark@chem.ethz.ch; Fax: +41 44 633 10 83; Tel: +41 44 632 09 80

† Electronic supplementary information (ESI) available: schematic showing both the original flame spray set up used for run 4 and the modified reducing flame spray set-up used for runs 1–3. See DOI: 10.1039/b601013j

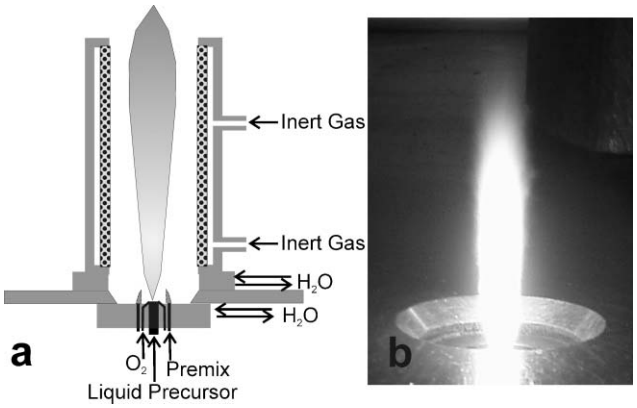

Fig. 1 Enclosure of a flame spray reactor in a porous metal tube allowed confinement of the flame reactor (a). Open flame burning in a N_2–H_2–CO atmosphere (b).

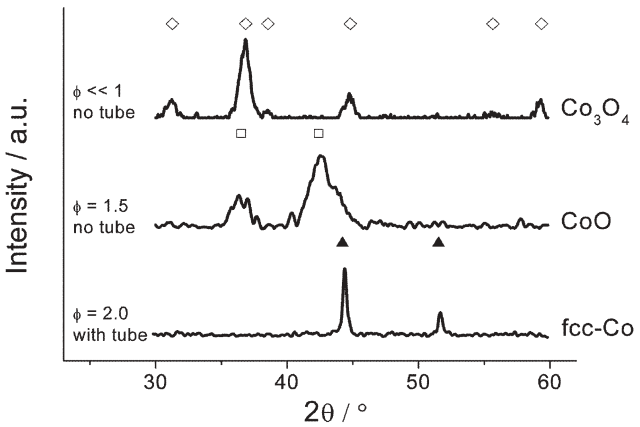

Fig. 2 X-Ray diffraction patterns of the as-produced powders using conventional flame synthesis (top trace). Reducing flame spray synthesis at ϕ = 1.5 (middle trace) and at ϕ = 2 using a sinter metal tube for cooling the flame (bottom trace). (◇: Co_3O_4 ($Fd\bar{3}m$); □ CoO ($Fm\bar{3}m$); ▲ fcc-Co ($Fm\bar{3}m$)).

the box (see ESI†). A sinter metal tube (GKN Sintermetalle, inner diameter 25 mm) surrounding the flame (Fig. 1a) allowed radial inflow of an inert mixing gas (PanGas, CO_2 or N_2, 99.995%) at a flow rate of 25 l min^{-1} and stable combustion. A mass spectrometer (Balzers, GAM 400) was applied for the detection of the gas concentrations of H_2, N_2, CO_2, NO, NO_2 and O_2. A separate data acquisition and control unit allowed controlling of the mass spectrometer, the liquid feed pump, mass flow controllers (Brooks) for sheath, dispersion and ignition gases as well as temperature of the box atmosphere and the adsorption columns. An oxygen concentration of below 100 ppm (volume/volume) was maintained during all experiments performed in the glove-box. The dispersion, ignition and combustion of the Co carboxylate based precursor was performed in the same way as the original flame spray set-up. While keeping a constant dispersing oxygen flow rate (5 l min^{-1}) the liquid flow rate was changed from 4.5 ml min^{-1} (for ϕ = 1.5) to 6 ml min^{-1} (for ϕ = 2).

For all experiments the fuel to oxygen ratio is defined as:[26]

$$\phi = \frac{\text{moles of } O_2 \text{ required for complete combustion}}{\text{moles of } O_2 \text{ supplied}} \quad (1)$$

where the moles of O_2 supplied account for all oxygen available for combustion and include the feed stream as well as oxygen from entrained gas.

Powder analysis

The nanoparticles were analyzed by X-ray diffraction (Siemens powder X-ray diffractometer with Ni-filtered CuK_α radiation, step size 0.3°), transmission electron microscopy (CM30 ST-Philips, LaB_6 cathode, operated at 300 kV, point resolution ~2 Å), scanning electron microscopy (LEO 1530 Gemini, Accelerating voltage 10 kV), magnetic hysteresis susceptibility (Quantum Design, Physical Property Measurement System) and thermal gravimetric analysis (Mettler Toledo SDTA851[e], 25–500 °C, 10 °C min^{-1}). The carbon content was measured by microanalysis (LECO, CHN-900).

Nitrogen adsorption was performed on a Tristar (Micromeritics Instruments) after sample pre-treatment under vacuum at 150 °C during 1 h. The mean particle diameter d_{BET} (Table 1) was calculated from the specific surface area (SSA_{N2}) and the material bulk density (ρ) using the following correlation:[26]

$$d_{BET} = \frac{6}{SSA_{N2}\rho} \quad (2)$$

Results and discussion

Continuous production of metallic cobalt nanoparticles

Under ambient conditions (in air: $\phi \ll 1$, run 4) conversion of cobalt 2-ethylhexanoate in a conventional spray flame yielded cobalt(II,III) oxide nanoparticles (Fig. 2, 1st trace). In a glove-box filled with nitrogen the flame reactor (Fig. 1b) could be operated at fuel rich conditions with ϕ up to 1.5 (reduced flame spray synthesis). The N_2 atmosphere allowed complete control of the amount of oxygen supplied to the combustion process. The nanoparticles produced under these conditions (run 3)

Table 1 Synthesis conditions and metallic nanoparticle properties

Run	Synthesis conditions	$c(O_2)$[a] (ppm)	ϕ[b]	XRD[c]	O_2 uptake[d] (wt%)	C[e] (wt%)	d_{BET}[f]/nm	d_{XRD}[g]/nm
1	CO_2	<100	2.0	Co (fcc)	31.5	0.4	54	20
2	N_2	<100	2.0	Co (fcc)	30	0.5	35	18
3	no tube/N_2	<100	1.5	CoO[h]	—	4	—	(4)[h]
4	no tube/Air	21%	≪1	Co_3O_4	<0.5	0.2	11	10

[a] Oxygen content in the flame off-gas (volume/volume). [b] Fuel to oxygen ratio. [c] Predominant crystal phase by X-ray diffraction (Fig. 2). [d] As determined by thermo-gravimetric analysis. [e] Carbon content as measured by microanalysis. [f] Particle size calculated from the specific surface area,[26] error ±10%. [g] Mean crystallite size as detected by XRD using the Scherrer formula.[27] [h] Mainly amorphous (see Fig. 2, 2nd trace)

were not metallic but consisted of reduced cobalt(II) oxide as shown by X-ray diffraction (Fig. 2, 2nd trace). The reduced oxide contained considerable amounts of solid carbonaceous species in the product (4 wt%, Table 1). Further increasing the fuel to oxygen ratio resulted in increasingly unstable flames. Incomplete conversion of the provided oxygen was evidenced by oxygen remainders in the off-gas. This observation may be attributed to incomplete mixing of fuel and oxygen within the reaction zone. Extensive formation of soot and measurable amounts of methane ($\sim$1 vol%) in the off-gas corroborated a lack of oxygen in some parts of the reaction zone and further supported the assumption of insufficient mixing. In order to better confine and mix the reactants within a highly turbulent reaction zone, the flame was encased in a sinter-metal tube (Fig. 1a). The porous tube allowed radial inflow of inert gases thus preventing particle deposition on the tube. This modified flame reactor could be operated at up to ϕ = 2. Stable conversion of the fuels (2-ethylhexanoic acid and tetrahydrofuran) and oxygen to a mixture of H_2, CO, CO_2 and water reduced the O_2 concentration in the off-gas to below 100 ppm. Using a cobalt carboxylate solution as fuel, metallic cobalt nanoparticles (Fig. 2, 3rd trace) could be produced at 30 g h^{-1} while avoiding the formation of undesired soot (carbon content $<$0.5 wt%, Table 1). While the detailed role of the chemical reactivity of the mixing gas requires further investigation, the larger particle size d_{BET} of cobalt nanoparticles prepared using CO_2 (run 1, Table 1) as a mixing gas in comparison to using N_2 (run 2, Table 1) indicated different oxidation and sintering behaviour during BET sample preparation.

Powder collected on a glass fiber filter from the off gas of a flame operated under these highly reducing conditions was light-weight and displayed excellent air stability (run 1, Table 1). Fig. 3a shows a scanning electron microscopy (SEM) image of the products displaying nearly spherical, slightly agglomerated nanoparticles with a primary particle diameter ranging from about 20–60 nm. The particle size distribution evaluated by particle counting (Fig. 3b) could be fitted to a log-normal distribution with a number based geometric standard deviation $\sigma_{g,n}$ of 1.5 $\pm$ 0.03.

The X-ray diffraction pattern of the cobalt powder (Fig. 2, bottom trace) showed the formation of face-centered-cubic (fcc) cobalt and no evidence of the formation of the thermodynamically favoured hexagonal-closed-packed (hcp) cobalt[28] or crystalline oxidic species. Particle size further correlated to the crystal size as determined from the peak width using the Scherrer formula.[27] The mean crystallite diameter as determined from the XRD pattern d_{XRD} (Table 1) was smaller than the mean particle size observed visually from SEM image analysis (Fig. 3). The difference may be attributed to the formation of polycrystalline particles or the formation of twins. The particle size calculated from nitrogen adsorption (d_{BET}) overestimated the actual, visually determined particle size which has been attributed to micropores between adhering nanoparticles[29] (see Fig. 4).

The thermal stability and oxygen uptake of the cobalt nanoparticles were measured in a thermobalance. The mass profile (Fig. 5) showed that the cobalt nanopowder was stable under air up to about 150 °C where it ignited (mass gain of about 17%) followed by a slow oxidation to a total mass gain of 31.5%. The surface of the particles was investigated by transmission electron microscopy (TEM, Fig. 4) and showed crystalline spheres with an amorphous edge of about 1 nm thickness. The metallic particles also showed stacking faults as previously reported for nanocrystalline fcc-cobalt.[30]

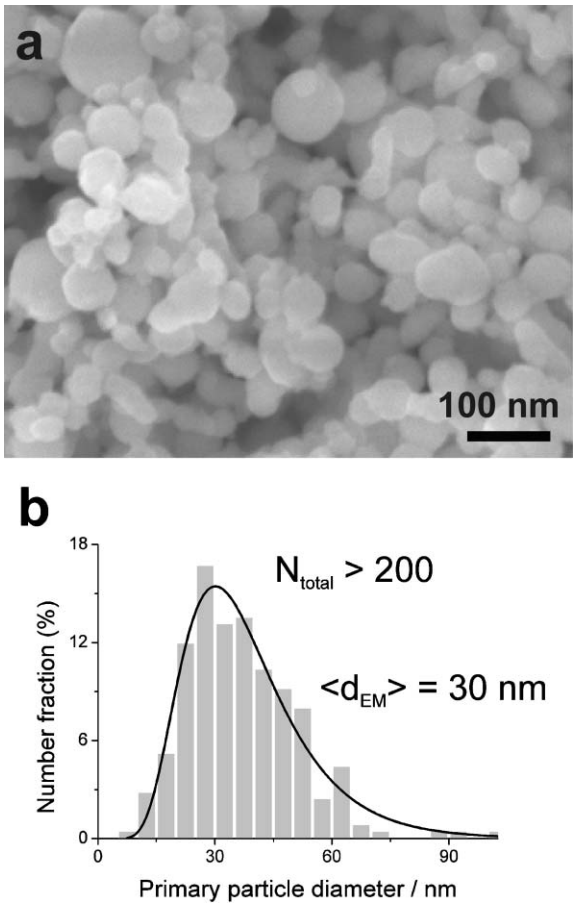

Fig. 3 Scanning electron microscopy (SEM) image of the cobalt particles after synthesis (a). Counted particle size distribution (b) with a fitted narrow log-normal distribution (line).

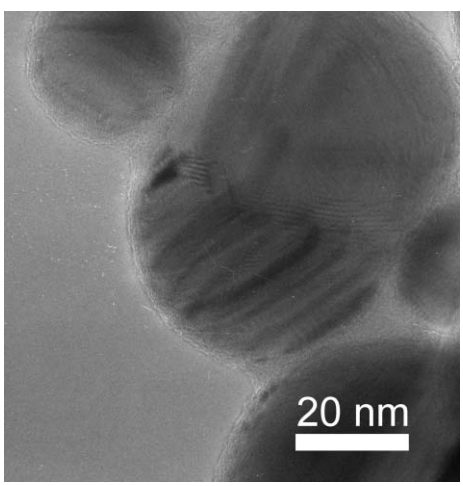

Fig. 4 High resolution transmission electron micrograph of the as-prepared metallic cobalt nanopowder.

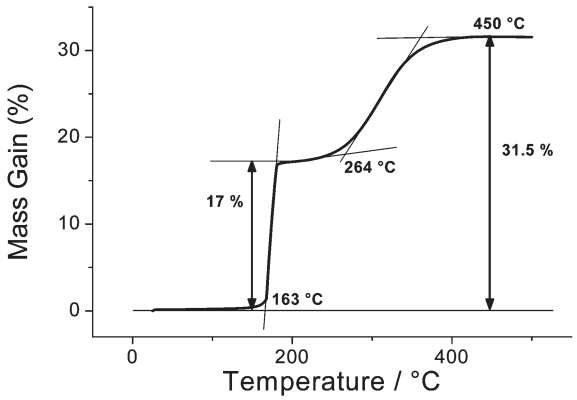

Fig. 5 Cobalt nanopowder mass gain upon oxidation measured by thermogravimetry.

The composition of the cobalt nanoparticles may be discussed in terms of the oxidation profile (Fig. 5), the surface structure (Fig. 4) and the saturation magnetisation (Fig. 6). From the thermogravimetric data the metallic content of the nanoparticles can be computed assuming full oxidation of cobalt metal to Co_3O_4 (theoretical mass gain of 36.2 wt%) and the measured values. This resulted in a calculated metal content of 87 wt%. A very low carbon content (Table 1; 0.4 wt%) may be attributed to adsorbed gaseous carbon species (CO, CO_2) and is insufficient to account for a carbon layer (monolayer: ~2 wt% carbon) covering the individual particles. The presence of oxides on the surface may explain the reduced oxygen uptake in thermogravimetry (Fig. 5) and the air stability up to 150 °C. Two–four monolayers of $CoO_{1.33}$ (~4–8 wt%) covering the metallic cobalt would explain the diminished mass gain. This interpretation is supported by transmission electron microscopy (Fig. 4) showing an amorphous layer of about 1 nm thickness covering the individual crystalline particles.

Fig. 6 shows the magnetic hysteresis loops of the as-prepared material recorded at 298 and 100 K. Both loops

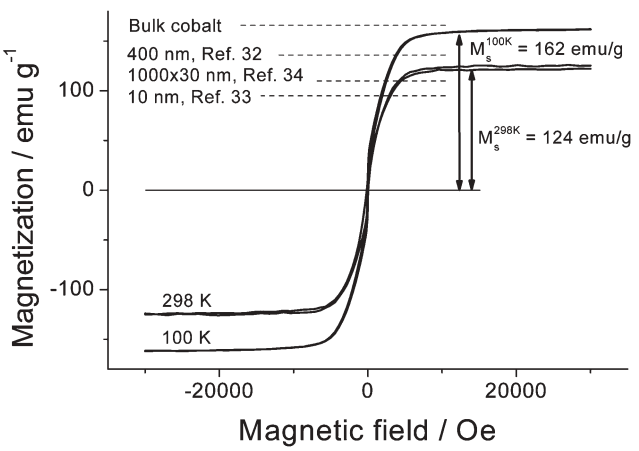

Fig. 6 Magnetic hysteresis of as-prepared cobalt nanopowder measured at 298 K or 100 K exhibiting a small coercivity and a large saturation magnetization (124–162 emu g^{-1}). Broken lines show reference saturation magnetizations for bulk cobalt,[31] cobalt nanoparticles[32,33] and cobalt platelets.[34]

showed a very small coercivity (<100 Oe) together with a high saturation magnetisation. While the saturation magnetisation at 298 K of 124 emu g^{-1} lay below the reference value for bulk cobalt metal (163–164 emu g^{-1}), at 100 K the saturation magnetisation was within 98% of the reference value (164–165 emu g^{-1}).[31] The saturation magnetisation at room temperature was similar or enhanced, compared to recent publications on nano-scaled cobalt materials[32–34] (see reference values in Fig. 6) favouring the use of the present material for magnetic applications.

A further measure for the purity of the sample was provided by the mass weighted saturation magnetisation taken from magnetic hysteresis loops (Fig. 6). The data at 100 K suggested a high content of magnetic cobalt (>90%). The reduced saturation magnetisation at 298 K indicated a strongly temperature dependent magnetic response and a reduced Curie temperature which agrees with prior observations on ultra-thin cobalt films.[35] The measured low coercivity (<100 Oe) was found to be characteristic for single domain magnetisation well below the critical single cobalt domain size of 70 nm[36] and is in agreement with the counted particle size distribution (Fig. 3b). The log-normal shape of the particle size distribution as well as the number based geometric standard deviation ($\sigma_{g,n}$) are in close agreement with modelling results[37] based on Brownian aggregation of nanoparticles in the gas phase (theoretical value $\sigma_{g,n}$ = 1.46, spheres, free molecular regime).

The results presented here show that the degree of reduction of the formed material can be controlled by the fuel to oxygen ratio. While at a low fuel to oxygen ratio cobalt(II,III) oxide was formed, an increased fuel to oxygen ratio resulted in the formation of cobalt(II) oxide. Further increasing the fuel to oxygen ratio finally resulted in the formation of metallic cobalt nanoparticles. In order to achieve full combustion at these fuel rich conditions the reaction had to be controlled by encasing the flame in a sinter-metal tube. It is believed that enhanced mixing of fuel and oxidizer and the increased reaction temperature in the sinter-metal tube allow for a more homogeneous combustion avoiding both the formation of soot and a higher oxygen yield. It is assumed that the formation of thin layers of cobalt oxide on the metallic particles can be ascribed to oxidation of the cobalt core by water or CO_2 during the cooling of the flame.

Equilibrium gas composition during reducing flame synthesis

Assuming equilibrium conditions the thermodynamic gas composition could be calculated using the following three independent gas phase reactions:

$$CH_4 + O_2 \leftrightarrow 2H_2 + CO_2 \quad (3)$$

$$CO_2 + H_2 \leftrightarrow CO + H_2O \quad (4)$$

$$2H_2 + O_2 \leftrightarrow 2H_2O \quad (5)$$

In this simplified case the fuel was assumed to consist of purely methane (CH_4) instead of the higher hydrocarbons used in the experiments. The calculated gas compositions (Fig. 7) clearly showed a large influence of the fuel to oxygen ratio on the combustion products at high temperatures (>1200 K). In the

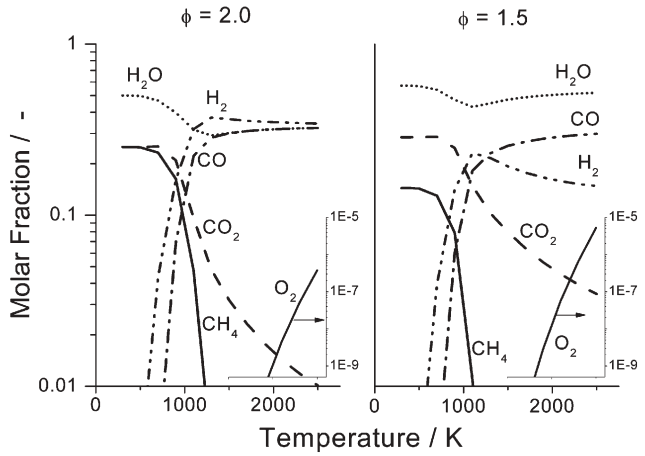

Fig. 7 Equilibrium gas composition calculated from reactions (3)–(5) as a function of temperature for $\phi = 2$ (left) and $\phi = 1.5$ (right).

case of $\phi = 2$ (left) the combustion products consisted of a near equimolar amount of H_2, H_2O and CO with only traces of CO_2. Lowering the fuel to oxygen ratio to $\phi = 1.5$ resulted in a strong increase of the oxidising species (H_2O and CO_2) together with a decrease of reducing species (H_2 and CO). These results were consistent with flame off-gas analysis performed by mass spectroscopy. With the use of an Ellingham diagram[38] it can be concluded that at high temperatures (>1000 K) both flames were reducing enough for the manufacture of metallic cobalt. Upon cooling the metallic form becomes less favourable in the case of the lower fuel to oxygen ratio and CoO is formed presumably through reaction with abundant water or CO_2 (Fig. 7, right). The measurements of increased water and CO_2 concentrations in the flame off-gas by mass spectroscopy assist this assumption. The calculations presented here however can only be used as very qualitative guidelines since real flames are not at thermodynamic equilibrium and do exhibit very strong kinetic and mixing effects.[39]

Conclusion

Highly air stable, face-centered-cubic cobalt nanoparticles were prepared by a modified flame spray based preparation method at up to 30 g h^{-1}. Nanoparticles of a mean diameter of $\sim$30 nm exhibited a narrow size distribution with a geometric standard deviation $\sigma_{g,n}$ of $\sim$1.5. The cobalt nanoparticles were covered with a thin layer of cobalt oxide protecting the material from oxidation in air. The use of fuel rich flames and a sinter-metal tube for enhanced gas mixing during the reaction gave rise to highly reducing conditions favouring the formation of metallic cobalt. In addition, reducing flame synthesis may further give access to the cost-efficient nanoparticle preparation of metals and alloys for use in electronic or magnetic applications.

Acknowledgements

The authors thank Dr F. Krumeich for transmission electron microscopy imaging and Alois Weber for conducting magnetic susceptibility measurements. This work has been supported by the CTI grant No. 7103.1 NMS-NM.

References

1 Q. Yan, T. Kim, A. Purkayastha, P. G. Ganesan, M. Shima and G. Ramanath, *Adv. Mater.*, 2005, **17**, 2233; H. Q. Li and F. Ebrahimi, *Adv. Mater.*, 2005, **17**, 1969.
2 G. A. Held and G. Grinstein, *Appl. Phys. Lett.*, 2001, **79**, 1501; E. I. Cooper, C. Bonhote, J. Heidmann, Y. Hsu, P. Kern, J. W. Lam, M. Ramasubramanian, N. Robertson, L. T. Romankiw and H. Xu, *IBM J. Res. Dev.*, 2005, **49**, 103.
3 G. Boero, I. Utke, T. Bret, N. Quack, M. Todorova, S. Mouaziz, P. Kejik, J. Brugger, R. S. Popovic and P. Hoffmann, *Appl. Phys. Lett.*, 2005, 86; A. Sandhu, K. Kurosawa, M. Dede and A. Oral, *Jpn. J. Appl. Phys., Part 1*, 2004, **43**, 777.
4 B. H. Lee, Y. J. Lee, K. H. Min, D. G. Kim and Y. D. Kim, *Mater. Lett.*, 2005, **59**, 3156.
5 A. T. Bell, *Science*, 2003, **299**, 1688; L. Guczi, *Catal. Today*, 2005, **101**, 53.
6 J. R. Thomas, *J. Appl. Phys.*, 1966, **37**, 2914.
7 V. F. Puntes, K. M. Krishnan and A. P. Alivisatos, *Science*, 2001, **291**, 2115.
8 V. Salgueirino-Maceira, M. A. Correa-Duarte, M. Farle, M. A. Lopez-Quintela, K. Sieradzki and R. Diaz, *Langmuir*, 2006, **22**, 1455; E. Barea, X. Batlle, P. Bourges, A. Corma, V. Fornes, A. Labarta and V. F. Puntes, *J. Am. Chem. Soc.*, 2005, **127**, 18026; S. M. Park, W. Ki, J. Yu and H. Du, *J. Mater. Res.*, 2005, **20**, 3094; M. Green, *Chem. Commun.*, 2005, 3002; J. Connolly, T. G. St Pierre, M. Rutnakornpituk and J. S. Riffle, *J. Phys. D: Appl. Phys.*, 2004, **37**, 2475; H. T. Yang, Y. K. Su, C. M. Shen, T. Z. Yang and H. J. Gao, *Surf. Interface Anal.*, 2004, **36**, 155; D. P. Dinega and M. G. Bawendi, *Angew. Chem., Int. Ed.*, 1999, **38**, 1788.
9 D. E. Rosner, *Ind. Eng. Chem. Res.*, 2005, **44**, 6045.
10 M. Mange, F. Chatelut and C. Eyraud, *J. Appl. Chem. Biotechnol.*, 1977, **27**, 236.
11 R. M. Laine, J. Marchal, H. P. Sun and X. Q. Pan, *Adv. Mater.*, 2005, **17**, 830.
12 F. E. Kruis, H. Fissan and A. Peled, *J. Aerosol Sci.*, 1998, **29**, 511; R. Riddle and M. Kuntz, *US Pat.*, 5.814.585, 1998; J. H. Brewster and T. T. Kodas, *AIChE J.*, 1997, **43**, 2665; M. R. Zachariah and S. Huzarewicz, *Combust. Flame*, 1991, **87**, 100.
13 T. Johannessen, J. R. Jenson, M. Mosleh, J. Johansen, U. Quaade and H. Livbjerg, *Chem. Eng. Res. Des.*, 2004, **82**, 1444; W. J. Stark, S. E. Pratsinis and A. Baiker, *J. Catal.*, 2001, **203**, 516; W. J. Stark, K. Wegner, S. E. Pratsinis and A. Baiker, *J. Catal.*, 2001, **197**, 182.
14 H. D. Jang, D. W. Hwang, D. P. Kim, H. C. Kim, B. Y. Lee and I. B. Jeong, *Mater. Res. Bull.*, 2004, **39**, 63; M. Ullmann, S. K. Friedlander and A. Schmidt-Ott, *J. Nanopart. Res.*, 2002, **4**, 499; B. Xia, I. W. Lenggoro and K. Okuyama, *J. Mater. Sci.*, 2001, **36**, 1701; K. Nagashima, T. Himeda and A. Kato, *J. Mater. Sci.*, 1991, **26**, 2477; B. Giesen, H. R. Orthner, A. Kowalik and P. Roth, *Chem. Eng. Sci.*, 2004, **59**, 2201; A. G. Nasibulin, P. P. Ahonen, O. Richard, E. I. Kauppinen and I. S. Altman, *J. Nanopart. Res.*, 2001, **3**, 385; D. Jang and D. Kim, *Appl. Phys. A*, 2004, **79**, 1985; J. C. Weigle, C. C. Luhrs, C. K. Chen, W. L. Perry, J. T. Mang, M. B. Nemer, G. P. Lopez and J. Phillips, *J. Phys. Chem. B*, 2004, **108**, 18601; W. H. Suh and K. S. Suslick, *J. Am. Chem. Soc.*, 2005, **127**, 12007.
15 R. Mueller, R. Jossen, S. E. Pratsinis, M. Watson and M. K. Akhtar, *J. Am. Ceram. Soc.*, 2004, **87**, 197.
16 W. J. Stark, L. Madler, M. Maciejewski, S. E. Pratsinis and A. Baiker, *Chem. Commun.*, 2003, 588.
17 S. Loher, W. J. Stark, M. Maciejewski, A. Baiker, S. E. Pratsinis, D. Reichhardt, F. Maspero, F. Krumeich and D. Günther, *Chem. Mater.*, 2005, **17**, 36; M. Huber, W. J. Stark, S. Loher, M. Maciejewski, F. Krumeich and A. Baiker, *Chem. Commun.*, 2005, 648.
18 R. N. Grass and W. J. Stark, *Chem. Commun.*, 2005, 1767.
19 H. Keskinen, J. M. Makela, M. Vippola, M. Nurminen, J. Liimatainen, T. Lepisto and J. Keskinen, *J. Mater. Res.*, 2004, **19**, 1544.
20 W. J. Stark and S. A. Pratsinis, *World Pat.*, 2004/103900 A1, 2004.

21 A. Moisala, A. G. Nasibulin and E. I. Kauppinen, *J. Phys.: Condens. Matter*, 2003, **15**, S3011.
22 J. M. Makela, H. Keskinen, T. Forsblom and J. Keskinen, *J. Mater. Sci.*, 2004, **39**, 2783.
23 R. L. Vander Wal, T. M. Ticich and V. E. Curtis, *Chem. Phys. Lett.*, 2000, **323**, 217.
24 M. J. Height, J. B. Howard, J. W. Tester and J. B. V. Sande, *Carbon*, 2004, **42**, 2295.
25 E. K. Athanassiou, R. N. Grass and W. J. Stark, *Nanotechnology*, 2006, **17**, 1668.
26 L. Madler, H. K. Kammler, R. Mueller and S. E. Pratsinis, *J. Aerosol Sci.*, 2002, **33**, 369.
27 H. Borchert, E. V. Shevehenko, A. Robert, I. Mekis, A. Kornowski, G. Grubel and H. Weller, *Langmuir*, 2005, **21**, 1931.
28 C. G. Granqvist and R. A. Buhrman, *J. Appl. Phys.*, 1976, **47**, 2200.
29 V. G. Kravets, C. Meier, D. Konjhodzic, A. Lorke and H. Wiggers, *J. Appl. Phys.*, 2005, 97.
30 M. E. McHenry, S. A. Majetich, J. O. Artman, M. Degraef and S. W. Staley, *Phys. Rev. B*, 1994, **49**, 11358.
31 R. Pauthenet, *J. Appl. Phys.*, 1982, **53**, 8187.
32 H. Tokoro, S. Fujii and T. Oku, *J. Magn. Magn. Mater.*, 2005, **290**, 141.
33 T. Hayashi, S. Hirono, M. Tomita and S. Umemura, *Nature*, 1996, **381**, 772.
34 H. G. Li, Y. Qin, X. L. Kou, H. Y. He and D. K. Song, *Mater. Lett.*, 2004, **58**, 2506.
35 C. M. Schneider, P. Bressler, P. Schuster, J. Kirschner, J. J. Demiguel and R. Miranda, *Phys. Rev. Lett.*, 1990, **64**, 1059.
36 D. L. LesliePelecky and R. D. Rieke, *Chem. Mater.*, 1996, **8**, 1770.
37 P. J. Dekkers and S. K. Friedlander, *J. Colloid Interface Sci.*, 2002, **248**, 295.
38 S. I. Sandler, *Chemical and Engineering Thermodynamics*, 3rd edn, John Wiley & Sons, New York, 1999.
39 A. Brink, P. Kilpinen, M. Hupa and L. Kjaldman, *Combust. Sci. Technol.*, 1999, **141**, 59.

